doi:10.3772/j.issn.1006-6748.2018.01.002

A tunable passive mixer for SAW-less front-end with reconfigurable voltage conversion gain and intermediate frequency bandwidth①

Tao Jian (陶　健), Fan Xiangning②, Zhao Yuan
(Institute of RF&OE-ICs, School of Information Science and Engineering, Southeast University, Nanjing 210096, P. R. China)

Abstract

An adjustable mixer for surface acoustic wave (SAW)-less radio frequency (RF) front-end is presented in this paper. Through changing the bias voltage, the presented mixer with reconfigurable voltage conversion gain (VCG) is suitable for multi-mode multi-standard (MMMS) applications. An equivalent local oscillator (LO) frequency-tunable high-Q band-pass filter (BPF) at low noise amplifier (LNA) output is used to reject the out-of-band interference signals. Base-band (BB) capacitor of the mixer is variable to obtain 15 kinds of intermediate frequency (IF) bandwidth (BW). The proposed passive mixer with LNA is implemented in TSMC 0.18μm RF CMOS process and operates from 0.5 to 2.5GHz with measured maximum out-of-band rejection larger than 40dB. The measured VCG of the front-end can be changed from 5 to 17dB; the maximum input intercept point (IIP3) is 0dBm and the minimum noise figure (NF) is 3.7dB. The chip occupies an area of 0.44mm^2 including pads.

Key words: reconfigurable, radio frequency (RF) front-end, multi-mode multi-standard (MMMS), high-Q band-pass filter (BPF), cross-coupled common gate low noise amplifier (CC-CG LNA), CMOS

0 Introduction

Recently, various kinds of wireless communication standards for handset mobile terminals are emerging and the whole industry is making great effort to enable mobile terminals to support more and more communication applications[1]. As an integral part of mobile platform, the radio frequency (RF) front-end needs to be reconfigurable for cellular communications and short range communications such as wireless local area networks (WLAN). Conventional multi-mode multi-standard (MMMS) systems with a large number of surface acoustic wave (SAW) filters are cumbersome for commercial applications. Thus, studying SAW-less MMMS RF front-end becomes an important trend[2,3].

One way to implement SAW-less RF front-end is depicted in Fig. 1. Use a high Q impedance translation band-pass filter (BPF) by adopting a passive mixer following with a base-band (BB) low-pass filter (LPF). And the gain and intermediate frequency (IF) bandwidth (BW) should be adjusted for MMMS applications, which is a big challenge. Recently, some SAW-less RF front-ends have been reported, while the gain and IF BW of these designs are fixed[4-6]. The low noise amplifiers (LNAs) could be blocked by interference signals. Another front-end structure can adjust gain and IF BW by changing transimpedance amplifier (TIA)[7-9], while the operational amplifier of TIA needs quite large gain-bandwidth.

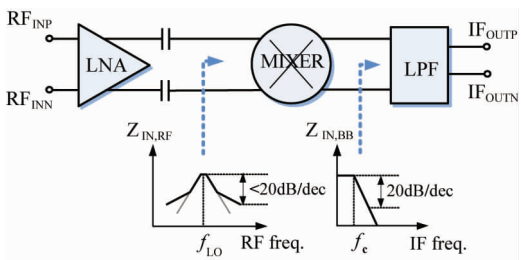

Fig. 1 Block diagram of a SAW-less RF front-end

In this paper, a tunable voltage-mode passive mixer is proposed with a cross-coupled common gate (CC-CG) LNA to handle interference signals. It can be flexibly reconfigurable in terms of VCG and IF BW performance, which is a great advantage for SAW-less MMMS RF front-end.

① Supported by the National Basic Research Program of China (No. 2010CB327404) and the Priority Academic Program Development of Jiangsu Higher Education Institutions.
② To whom correspondence should be addressed. E-mail: xnfan@seu.edu.cn
Received on Mar. 27, 2017

The paper is organized as follows. Section 1 discusses the high Q RF BPF based on passive mixer impedance translation model. Section 2 analyzes the design considerations for CC-CG LNA. In Section 3, a transistor-level of the SAW-less RF front-end is presented. The measurement results are shown in Section 4. Finally, conclusions are drawn in Section 5.

1 Tunable high-Q RF BPF based on passive mixer

A high-Q RF filter forms the core of the SAW-less RF front-end, and the main body is made of a pair of double balanced mixing switches as depicted in Fig. 2(a). This mixer can be used as an N-path filter if its output connects with a BB capacitor[10]. A 4-phase or 8- phase local oscillator (LO) would provide additional benefits in harmonic rejection and noise. However, 4-phase or 8-phase LO will increase power consumption and make the circuit design more complicated. For simplicity, the mixer of this study is driven by a 50% duty cycle LO.

1.1 Reconfiguration analysis

The LNA acts like a transconductance stage. In order to analyze the performance of high-Q RF BPF with LNA, the circuit is simplified in Fig. 2(b)[11]. Current $I_{RF}(\omega)$ flows out from LNA output which can be expressed as

$$I_{RF}(\omega) = G_{m,eff} \cdot V_{RF}(\omega) \tag{1}$$

where ω is RF angular frequency, $G_{m,eff}$ is the effective transconductance of LNA. Denote $Z_{RF}(\omega)$ as the output impedance of LNA, R_{SW} is the mixer switch on-resistance, $Z_{BB}(\Delta\omega)$ is the impedance of C_{BB}, η is the scaling factor for $Z_{BB}(\Delta\omega)$, and $Z_{sh}(\omega)$ represents the power dissipation due to BB signal re-up conversion to the RF side, which is expressed as

$$Z_{sh}(\Delta\omega) = \frac{4\eta}{1-4\eta}(R_{SW} + Z_{RF}(\Delta\omega)) \tag{2}$$

And the input impedance of the mixer is

$$Z_{MIX}(\Delta\omega) = R_{SW} + \eta Z_{BB}(\Delta\omega) // Z_{sh}(\omega) \tag{3}$$

where $\Delta\omega = \omega - \omega_{LO}$. Based on this, the output can be deduced:

$$\begin{aligned} V_{OUT}(\Delta\omega) &= I_{RF} \cdot (Z_{RF}(\omega) // Z_{MIX}(\omega)) \\ &\quad \cdot \frac{\eta Z_{BB}(\Delta\omega) // Z_{sh}(\omega)}{Z_{MIX}(\omega)} \\ &= \frac{4\eta G_{m,eff} Z_{BB}(\Delta\omega) Z_{RF}(\omega)}{Z_{BB}(\Delta\omega) + 4(R_{SW} + Z_{RF}(\omega))} V_{RF}(\omega) \end{aligned} \tag{4}$$

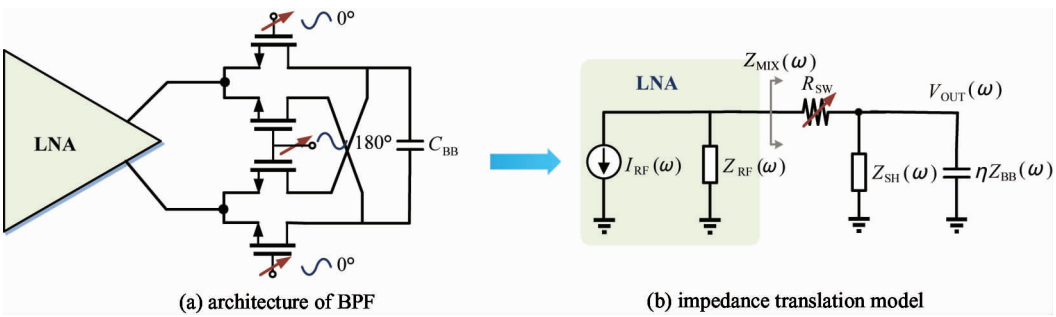

Fig. 2 High-Q RF BPF model with LNA

The following assumptions can be made for out-of-band interferers:

$$\Delta\omega >> BW/2 \rightarrow Z_{BB}(\Delta\omega) = \frac{1}{j\Delta\omega C_{BB}} << 4(R_{SW} + Z_{RF}(\omega)) \tag{5}$$

Therefore, the VCG for out-of-band interferers is simplified as

$$VCG(\omega) = \frac{V_{OUT}(\Delta\omega)}{V_{RF}(\omega)} \approx \frac{\eta G_{m,eff} Z_{RF}(\omega)}{(R_{SW} + Z_{RF}(\omega))} Z_{BB}(\Delta\omega) \tag{6}$$

where $Z_{RF}(\omega)$ is hardly changed around input frequency. So VCG is proportional to $Z_{BB}(\Delta\omega)$, that means the impedance of BB capacitor with LPF profile transfers a high-Q BPF at LNA output and the center of BPF is just at LO frequency (Fig. 3(a)). Furthermore, if the value of C_{BB} can be adjusted, the BW of BPF will change accordingly (Fig. 3(b)).

Worthy to mention that R_{SW} is only in the denominator of Eq. (4) and it doesn't affect other parameters. If the value of R_{SW} can be changed, the VCG could be reconfigured easily. The R_{SW} can be presented as

$$R_{SW} = \frac{1}{\mu_n C_{ox} \frac{W}{L}(V_{GS} - V_{TH})} \tag{7}$$

where w and L are the width and length of switching MOS transistor. V_{TH} is the threshold voltage; C_{OX}, the gate oxide capacitance per unit area; μ_n, the mobility of charge carriers and V_{GS} is gate-source voltage of the switching MOS. Therefor R_{SW} is controlled by V_{GS}. If

R_{SW} is reduced linearly by changing the gate voltage (VB_{LO}) of switching MOS, VCG will increase gradually (Fig. 3(c)).

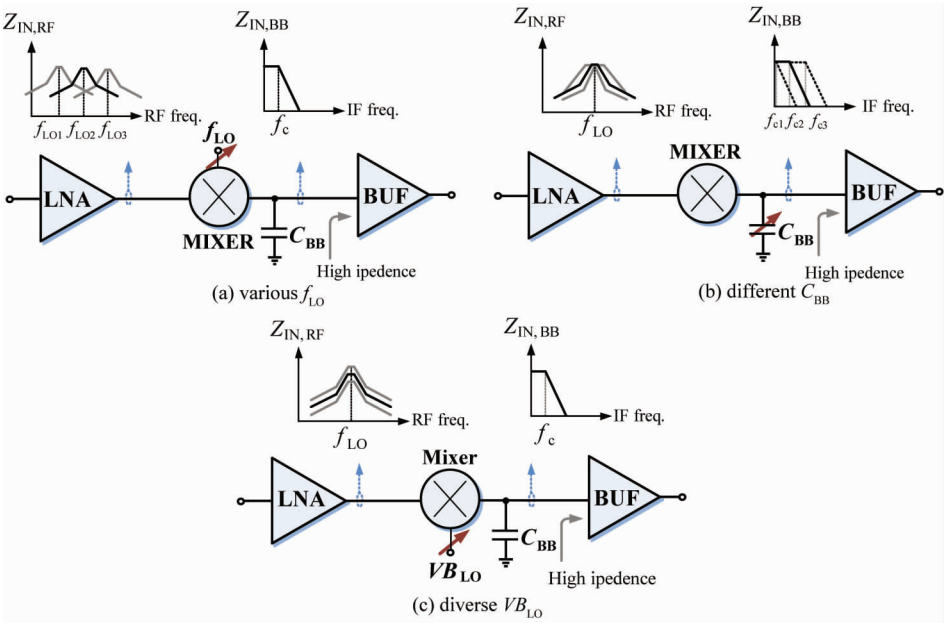

Fig. 3 High-Q RF filter characteristic under different conditions

Back to Fig. 2(b), the LNA gain can be obtained as follows:

$$A_{LNA}(\omega) = I_{RF} \cdot Z_{RF}(\omega) // Z_{MIX}(\omega) = I_{RF} \cdot Z_{RF}(\omega) // \left[R_{SW} + \frac{4\eta^2 (R_{SW} + Z_{BF}(\omega)) Z_{BB}(\Delta\omega)}{4\eta (R_{SW} + Z_{RF}(\omega)) + (\eta - 4\eta^2) Z_{BB}(\Delta\omega)} \right] \tag{8}$$

The following assumptions could be also made for in-band signal:

$$Z_{BB}(\Delta\omega) = \frac{1}{j\Delta\omega C_{BB}} >> \frac{4(R_{SW} + Z_{RF}(\omega))}{1 - 4\eta} \tag{9}$$

The LNA gain can be approximated as

$$A_{LNA}(\omega) \approx I_{RF} \cdot Z_{RF}(\omega) // \left[\frac{R_{SW}}{1 - 4\eta} + \frac{4\eta Z_{RF}(\omega)}{1 - 4\eta} \right] \tag{10}$$

It means that a small R_{SW} will decrease LNA gain and improve linearity due to smaller voltage swing at the output of LNA. Therefore, a small value of R_{SW} will results in a larger VCG and higher linearity, that is very critical.

1.2 Noise analysis

The noise sources are introduced in the architecture of the proposed high-Q RF BPF in Fig. 4. The thermal noise of source resistor R_S and mixer on-resistance R_{SW} are $4kTR_S$ and $4kTR_{SW}$ separately, where k denotes the Boltzmann constant and T is the absolute temperature. $\bar{I}^2_{n,\,LNA}$ is the noise current flows from LNA. The noise of mixer equivalent resistance is also white noise, so it will be down-converted by all the harmonics of the f_{LO} to baseband output. The noise of mixer at output is given by Ref. [10].

$$\bar{V}^2_{n,out\_mix} = 4kTR_{SW} \cdot \sum_{-\infty}^{+\infty} a_n \tag{11}$$

where a_n is the Fourier coefficient which depends on phase number of LO. Thus NF of the circuit from Fig. 4 can be obtained as

$$NF = 1 + \underbrace{\frac{\bar{I}^2_{n,\,LNA}}{kTR_S \cdot G^2_{m,eff}}}_{LNA} + \underbrace{\frac{\pi^2 R_{SW} \cdot \sum_{-\infty}^{+\infty} a_n}{4R_S \cdot G^2_{m,eff} \cdot (Z_{RF}(\omega) // Z_{MIX}(\omega))^2}}_{MIXER} \tag{12}$$

Same as Eq. (9), for in-band signal NF can be approximated to

$$NF \approx 1 + \frac{\bar{I}^2_{n,\,LNA}}{kTR_S \cdot G^2_{m,eff}} + \frac{\pi^2 R_{SW} \cdot \sum_{-\infty}^{+\infty} a_n}{4R_S \cdot G^2_{m,eff} \cdot (4\eta Z_{RF}(\omega))^2} \tag{13}$$

As Eq. (13) shown, the best way to reduce the noise is to increase $G_{m,eff}$. In addition, increasing the load of LNA and decreasing the parastic capacitor at LNA output also could improve the noise performance of the whole circuit.

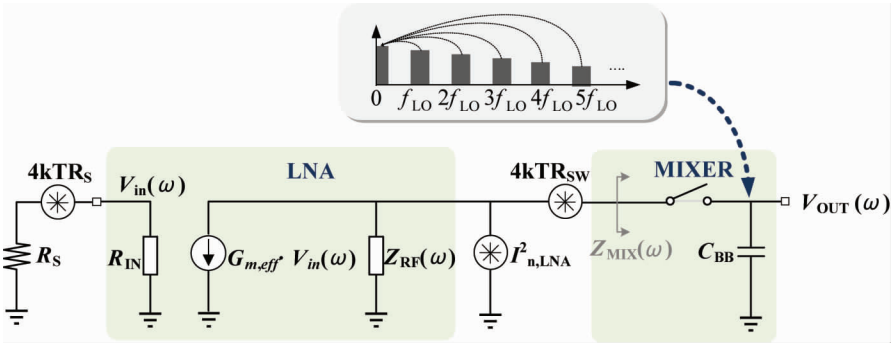

Fig. 4 The simplified circuit model with main noise sources

2 CC-CG LNA design

High-Q BPF works at LNA output. When out-of-band interference enters into LNA, it should not be amplified, otherwise the LNA will be blocked. CG LNA converts a voltage input signal to a current signal at output and interference can be filtered at LNA output.

CC-CG LNA is used in Fig. 5, because it has g_m boosted effect[12]. When $C_C \gg C_{gs}$, the effective transconductance $G_{m,eff} \approx 2g_{mi}$, where C_C, C_{gs} and g_{mi} are the cross-coupled capacitor, gate-to-source capacitor, transconductance of M_1 and M_2 respectively. The approximate NF of CC-CG LNA is

$$F_{CC\text{-}CG} \approx 1 + \frac{\gamma}{\alpha}\left(\frac{C_{gs}+C_C}{C_{gs}+2C_C}\right) + \frac{4R_S}{R_L} \approx 1 + \frac{\gamma}{2\alpha} + \frac{4R_S}{R_L} \quad (14)$$

And for traditional CG LNA

$$F_{CG} \approx 1 + \frac{\gamma}{\alpha} + \frac{4R_S}{R_L} \quad (15)$$

where γ and α are the bias-dependent noise parameters, R_S, source resistance, and R_L, load resistance. Hence, compared with traditional CG LNA, it has lower NF for the same power dissipation. Size and bias of M_1 and M_2 can be adjusted to achieve input matching. The perfect input matching conditions occurs at $R_s = 1/2g_{mi}$. Decreasing the input impedance, for example, to 30 Ω will result in $S_{11} \approx -12$dB, but g_{mi} increases to 16.7ms. That means higher gain and lower NF.

Another interesting characteristic of CC-CG LNA is that it can reduce second-order distortion. And its third order inter-modulation point is given[13]:

$$AIP3_{CC\text{-}CG} = \sqrt{8 \mid \frac{g_{mi}}{g''_{mi}}(2g_{mi}(Z_L//R_S)+1)^3 \mid} \quad (16)$$

where Z_L is the impedance of external inducter. Thus lager g_{mi} can also help to increase AIP3. In order to further boost compression point of LNA, a 2.5V supply voltage[14] is used. Make sure no device terminal suffers more than the reliability specification of the technology. L_{ext} is external choke inductance to offer DC path for LNA, and it can also eliminate the parasitic capacitor (C_{pad}) at input pad. Cascade devices M_3 and M_4 improve the reverse isolation. R_L can offer large output impedance over wide BW.

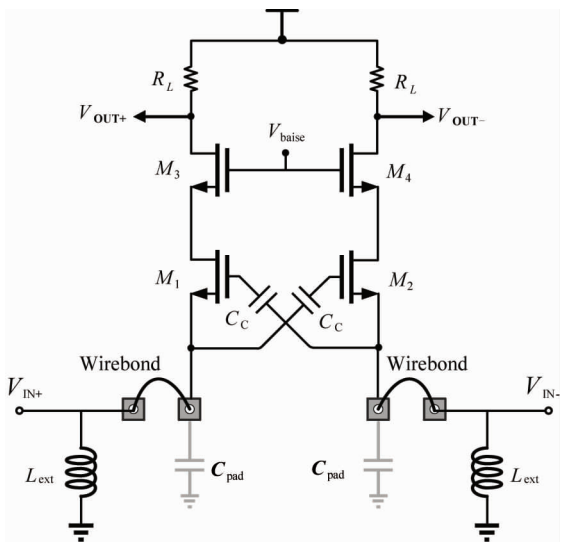

Fig. 5 Schematic of CC-CG LNA

3 Circuit implementation

The theoretical predictions are verified by implementing the passive mixer with CC-CG LNA in TSMC 0.18 μm RF CMOS technology. As explained in Section 2, the circuit is shown in Fig. 6. CC-CG LNA uses a pair of cross-coupling capacitor C_{C1} and C_{C2} to implement g_m boosting. Metal-insulator-metal capacitor is recommended that it makes less thermal noise than MOS capacitor. Differential transistors M_3 & M_4 are biased making g_{mi} = 16.7ms, which causes the input impedance to become 30Ω. It is a good compromise for matching and NF. Cascade devices M_1 and M_2 are added to improve the reverse isolation. L_1 and L_2 are off-

chip choke inductances to offer DC path. Supply voltage is lifted to 2.5V to compensate the voltage across resistance load R_{L1} and R_{L2}.

Mixer stage consists of a pair of double balanced mixing switches. One key issue is the size of switch transistors (M_5 – M_8). A high W/L ratio results in a small R_{SW}, and it would be beneficial to improve linearity and gain. Considering the input frequency of the mixer, the RF transistors implemented in the deep N-well are used as switches due to their attractive high frequency performance. Capacitor C_3 and C_4 are used for AC current coupling from LNA stage. Zero DC current of switch transistors improve the flicker noise performance. The IF BW must be reconfigurable for MMMS applications. A capacitor array is taken as C_{BB} which consists of four capacitors in parallel and each capacitor is controlled by digital signal. C_{BB} is various from 2pF to 46pF, and the value of BW is changed from 4MHz to 66MHz. As mentioned in part 2, the VCG is inverse to R_{SW}. The value of R_{SW} is determined by the gate bias voltage of switch transistors. If adjusting the VB_{LO} in constant then the VCG could be fine tuned. External LO is 0dBm sinusoidal signal which is transferred into a differential signal by off-chip balun.

The simple buffer is implemented for test. The common source stage with 60Ω resistance load can offer good matching at output. The gate of M_9 and M_{10} are high impedance that wouldn't affect the gain and BW.

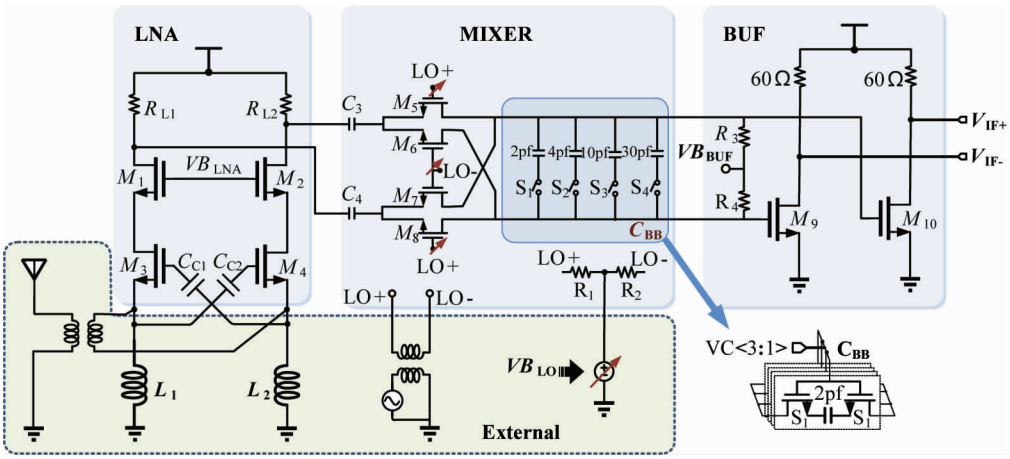

Fig. 6 Entire schematic of proposed front-end including buffer

4 Measurement results

The proposed circuit is fabricated in TSMC 0.18μm RF CMOS technology. Fig. 7 shows the chip photograph of the proposed circuit. The die area is 0.7mm × 0.63mm including pads. The measured DC current is 4.9mA from a 2.5V supply voltage. All measurements are performed using an assembled printed circuit board (PCB). RF signal are applied using a commercial wideband balun. The insertion loss from external components and transmission lines is measured at the desired frequencies and used for compensating the measurement results.

The VCG measurement is performed with the LO frequencies from 500MHz to 2.5GHz in double sideband in Fig. 8. With various f_{LO}, for example 1.5GHz, the IF BW is fixed at 4MHz and the frequency of input signal is changed from 1.5001GHz to 2GHz, so that the output IF frequency can be swept from near dc to 500MHz as high sideband VCG. Then the input signal is varied from 1G to 1.4999G to plot the low sideband VCG. The rejection is larger than 25dB at 100MHz offset frequency in the wideband range and the maximum rejection larger than 40dB.

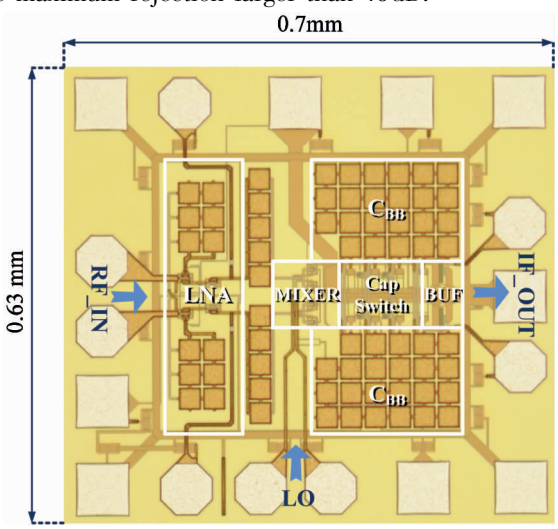

Fig. 7 Die micrograph of the test chip

The IF BW should be flexibly reconfigurable for multimode application. Fig. 9 shows the measured VCG with 1.5GHz LO frequency. The IF BW depends on the value of C_{BB} and it can be adjusted from 4MHz to 66MHz for different C_{BB}. This SAW-less RF front-end can offer 15 kinds of IF BW to adapt different communication standards.

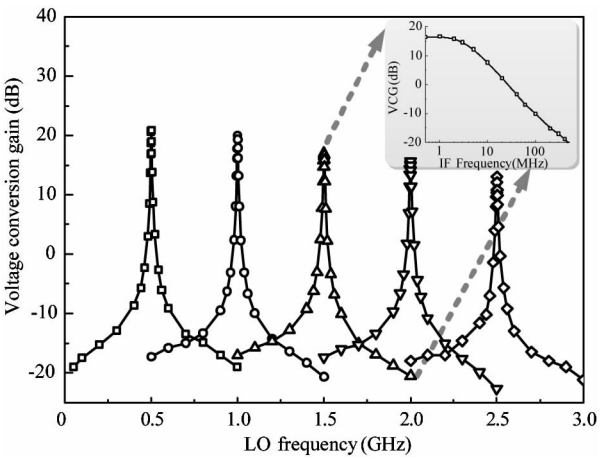

Fig. 8 Measured VCG curves of proposed circuit with different LO frequency

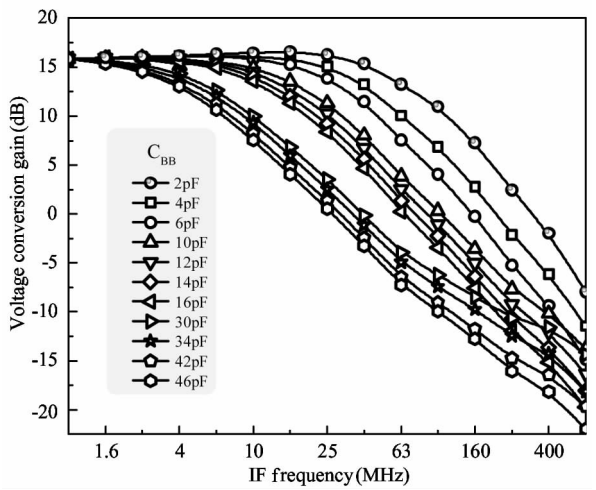

Fig. 9 Measured IF bandwidth with different C_{BB}

Fig. 10(a) shows measured 1-dB Compression curves at 4MHz IF BW (C_{BB} is 46pF) and 1.5GHz LO frequency. Then 1-dB Compression points are found under various offset frequencies ($\Delta f = f_{in} - f_{LO}$) to compare the variation of linearity. Fig. 10(b) depicts measured 1-dB compression points of 4 different IF BW. It clearly shows that the linearity of out-of-band is much better than in-band. So the circuit can resist higher interference signals at out-of-band frequencies.

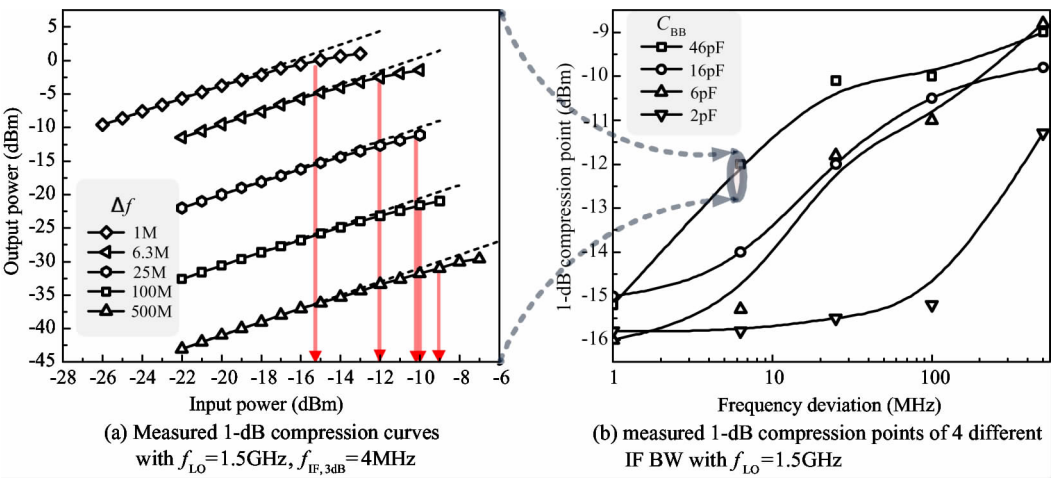

(a) Measured 1-dB compression curves with f_{LO}=1.5GHz, $f_{IF,3dB}$=4MHz

(b) measured 1-dB compression points of 4 different IF BW with f_{LO}=1.5GHz

Fig. 10 Measured 1-dB compression point

Since we are only interested in intermodulation products that fall in the channel band, measurements are carried out with the two tones located at frequency offsets Δf +600kHz and $2\Delta f$, such that the third-order intermodulation (IM3) always falls at 1.2MHz. Fig. 11 shows the measured IIP3 with a 1.5GHz LO and four different C_{BB}. IIP3 is measured for various Δf showing that with a larger C_{BB} engaged, the circuit could have better linearity under same interferers. With increasing Δf, the out-band IIP3 is improved to +0dBm.

In Section 3, the fact that different R_{SW} can affect the performance significantly is discussed. Fig. 12 depicts the measured results to verify this concept. By increasing the gate voltage of switch transistors (VB_{LO}), the R_{SW} can be decreased. Adjusting VB_{LO} from 0.95V to 1.3V with 1.5GHz LO frequency, the VCG is increased from 5dB to 17dB which is shown in Fig. 12(a). The noise performance is illustrated in Fig. 12(b) which has not much changed. The in-band IIP_3 and 1-dB compres-

sion point are shown in Fig. 12(c). They are improved almost 10dB from large R_{SW} to small R_{SW}.

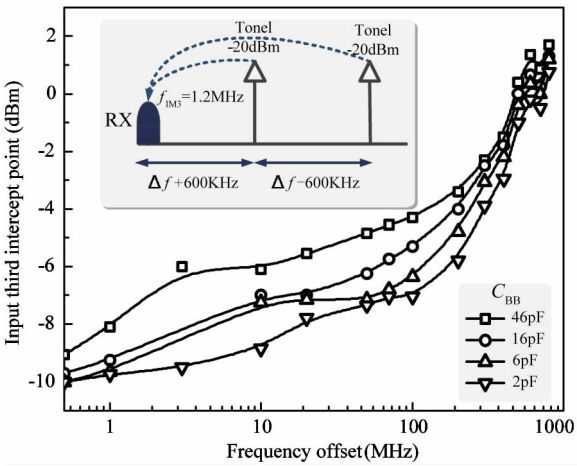

Fig. 11 Measured in-band and out-band IIP3 at 2GHz LO with four C_{BB} settings

Considering the wideband applications, the VCG, noise and in-band linearity are measured with varied LO frequency from 0.5GHz to 2.5GHz. Fig. 13(a) shows in-band VCG with different LO frequency. Due to parasitic at LNA the in-band VCG is falling from 21dB to 14dB. Fig. 13(b) illustrates the NF for different LO frequency. The NF is smaller than 5dB when LO frequency belows 1.5GHz and the deterioration of the noise is due to smaller gain. The in-band IIP_3 and 1-dB compression point is depicted in Fig. 13(c). Two tons with Δf = 500kHz are applied to the input of the LNA with power −20dBm. The maximum measured IIP_3 is larger than 0dB at 2.5GHz LO frequency and larger than −13dB for all frequencies. The measured 1-dB compression point shows similar trend to that of IIP_3 with respect to LO frequency.

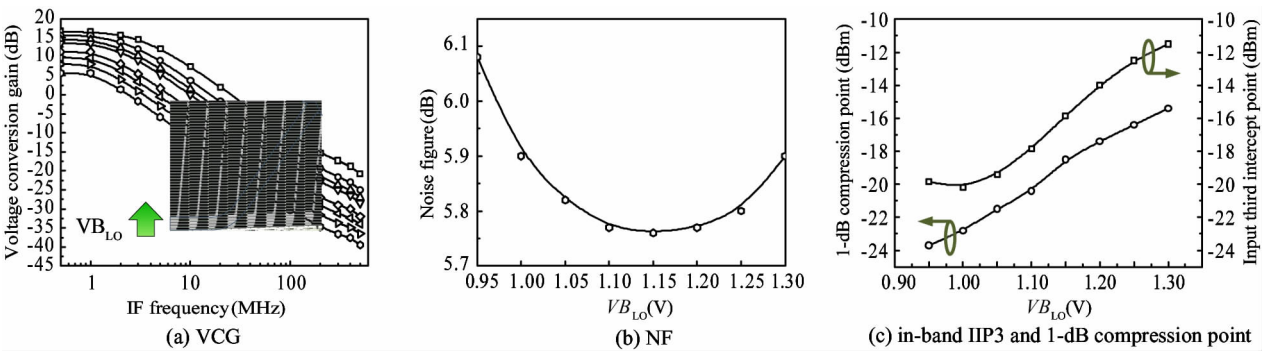

Fig. 12 Measured VCG, NF, in-band IIP3 and 1-dB compression point with f_{LO} = 1.5GHz, while the VB_{LO} is changed from 0.95V to 1.3V

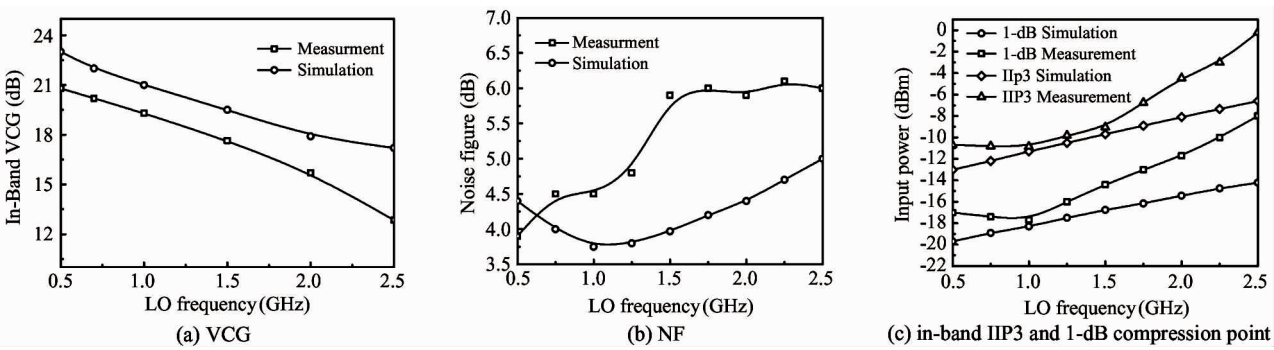

Fig. 13 Simulated and measured VCG, NF, in-band IIP3 and 1-dB compression point with different f_{LO}

The measured S_{11} and S_{22} are plotted in Fig. 14. As shown, S_{11} is less than −10dB from 0.5GHz to 2.5GHz which validates the broadband input matching. The measured S_{22} is also below −10dB over the frequency range of 10 − 100MHz.

Table 1 summarizes the measured results of the proposed circuit and gives a comparison with other recently published wideband front-ends.

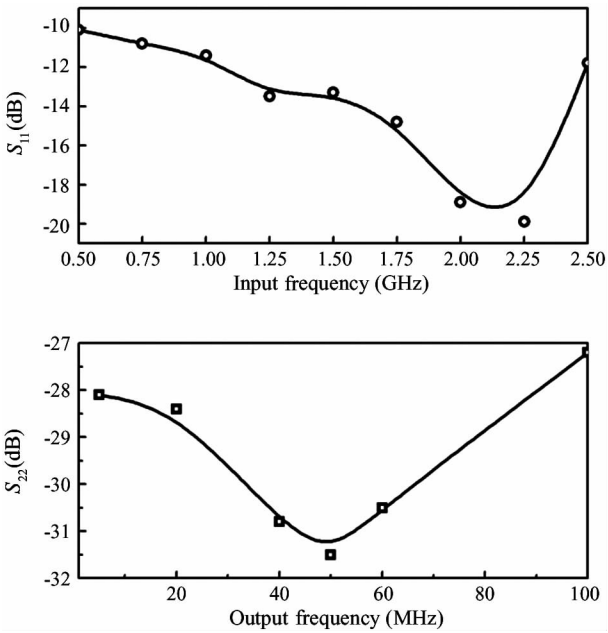

Fig. 14 Measured S_{11} and S_{22} of proposed circuit

5 Conclusion

This paper reports the design of a tunable mixer for multi-mode multi-standard (MMMS) applications, and the circuit is implemented in TSMC 0.18μm RF CMOS process. The adjustable mixer switches have been proposed in order to reconfigure the VCG flexibly. A LO frequency-tunable high-Q filter transfering at LNA output can reject out-of-band interferences. Furthermore the IF BW can be reconfigurable by using different C_{BB}. Measurement results indicate that the designed mixer can provide low NF and high linearity over wideband in the applications of MMMS wireless communications.

Table 1 Performance comparison

	The proposed work	ESSCIRC 2010[6]	J Semicond 2016[15]	TMTT 2010[16]	TMTT 2012[17]
Technology	0.18μm CMOS	90nm CMOS	0.18μm CMOS	0.18μm CMOS	0.13μm CMOS
RF frequency (GHz)	0.5 – 2.5	0.4 – 3	0.7 – 2.3	1.5 – 2.3	0.6 – 3
Gain (dB)	5 – 17	16	4 – 22	22.5 – 25	42 – 48
IF bandwidth (MHz)	3 – 66	10	12	NA	0.8 – 12
Min NF (dB)	3.7	2.8	8	7.7	3
Max IIP3(dBm)	0	11	8.5	8	– 14
Supply voltage(V)	2.5	2	1.8	1.8	1.2
Power(mW)	12.3	13	15	10	30
Note	LNA + Mixer	LNA + Mixer	LNTA + Mixer + TIA	LNTA + Mixer + TIA	LNTA + Mixer + TIA

References

[1] Lin F, Mak P, Martins R P. Wideband receivers: design challenges, tradeoffs and state-of-the-art [J]. *Circuits and Systems Magazine*, 2015, 13(1):12-24

[2] Madadi I, Tohidian M, Cornelissens K, et al. A high IIP2 SAW-less superheterodyne receiver with multistage harmonic rejection[J]. *IEEE Journal of Solid-State Circuits*, 2016, 51(2):332-347

[3] Murphy D, Darabi H, Xu H. A noise-cancelling receiver resilient to large harmonic blockers[J]. *IEEE Journal of Solid-State Circuits*, 2015, 50(6):1336-1350

[4] Hedayati H, Lau W A, Kim N, et al. A 1.8dB NF blocker-filtering noise-canceling wideband receiver with shared TIA in 40nm CMOS[J]. *IEEE Journal of Solid-State Circuits*, 2015, 50(5): 1148-1164

[5] Ostman K B, Englund M, Viitala O, et al. Analysis and design of N-path filter offset tuning in a 0.7 – 2.7GHz receiver front-end[J]. *IEEE Transactions on Circuits and Systems I: Regular Papers*, 2015, 62(1): 234-243

[6] Borremans J, Mandal G, Debaillie B, et al. A sub-3dB NF voltage-sampling front-end with +18dBm IIP3 and +2dBm blocker compression point[C]. In: Proceedings of the European Solid-state Circuits Conference, Sevilla, Spain, 2010. 402-405

[7] Yang D, Andrews C, Molnar A. Optimized design of N-phase passive mixer-first receivers in wideband operation[J]. *IEEE Transactions on Circuits and Systems I: Regular Papers*, 2015 62(11): 2759-2770

[8] Zhang X, Chi B, Wang Z. A 0.1 – 1.5 GHz harmonic rejection receiver front-end with phase ambiguity correc-

tion, vector gain calibration and blocker-resilient TIA [J]. *IEEE Transactions on Circuits and Systems I: Regular Papers*, 2015, 62(4): 1005-1014

[9] Nejedl A, Sjoland H, Tormanen M. A noise-cancelling receiver front-end with frequency selective input matching [J]. *IEEE Journal of Solid-State Circuits*, 2015, 50(5): 1137-1147

[10] Mirzaei A, Darabi H, Murphy D. Architectural evolution of integrated M-phase high-Q bandpass filters[J]. *IEEE Transactions on Circuits and Systems I: Regular Papers*, 2012, 59(1): 52-65

[11] Andrews C, Molnar A. A passive mixer-first receiver with digitally controlled and widely tunable RF interface[J]. *IEEE Journal of Solid-State Circuits*, 2010, 45(12): 2696-2708

[12] Zhou W, Li X, Shekhar S, et al. A capacitor cross-coupled common-gate low-noise amplifier[J]. *IEEE Transactions on Circuits and Systems II: Express Briefs*, 2005, 52(12): 875-879

[13] Han H G, Jung D H, Kim T W. A 2.88mW +9.06dBm IIP3 common-gate LNA with dual cross-coupled capacitive feedback[J]. *IEEE Transactions on Microwave Theory and Techniques*, 2015, 63(3):1019-1025

[14] Borremans J, Mandal G, Giannini V, et al. A 40 nm CMOS 0.4 – 6GHz receiver resilient to out-of-band blockers[J]. *IEEE Journal of Solid-State Circuits*, 2011, 46(7):1148-1164

[15] Fan X, Tao J, Bao K, et al. A reconfigurable passive mixer for multimode multistandard receivers in 0.18μm CMOS[J]. *Journal of Semiconductors*, 2016, 37(8): 085001 1-8

[16] Kim N, Aparin V, Larson L E. A resistively degenerated wideband passive mixer with low noise figure and high IIP_2 [J]. *IEEE Transactions on Microwave Theory and Techniques*, 2010, 58(4): 820-830

[17] Wang X, Sturum J, Yan N, et al. 0.6 – 3GHz wideband receiver RF front-end with a feedforward noise and distortion cancellation resistive-feedback LNA [J]. *IEEE Transactions on Microwave Theory and Techniques*, 2012, 60(2): 387-392

Tao Jian, born in 1985. He received the B. S. degree in electrical engineering from Hefei University of Technology, Hefei, China, in 2008, and M. S. degree from Xiamen University, Xiamen, China, in 2011. From 2011 to 2014, he has worked as RFIC engineer at GoldTel Group, Chengdu, China. He is currently pursuing the Ph. D. degree at Southeast University, Nanjing, China. His research interests include RF/analog circuits for wireless applications.